Fatigue Life Prediction Techniques for Polymers and Polymer Matrix Composites

Amir K. Shojaei[1]†, and Pieter Volgers[2]
[1]DuPont Performance Materials, Chestnut Run Plaza, Wilmington, DE, 19805, USA
[2]DuPont Performance Materials, European Technical Centre, CH-1217 Meyrin, Geneva, Switzerland
†Corresponding author
Email: Kian.A.Shojaei@DuPont.com,and A.Shojaei.Mech.Eng@gmail.com,
Tel: +1(302) 892-1182

ABSTRACT

To include the self-heating effect into the fatigue computation, information regarding hysteresis energy is required. As shown in Fig. 1, the hysteresis energy can be calculated by subtracting strain energies during the loading W_L and unloading W_U event. The calculated hysteresis energy includes information regarding both plastic deformation together with damage induced dissipations.

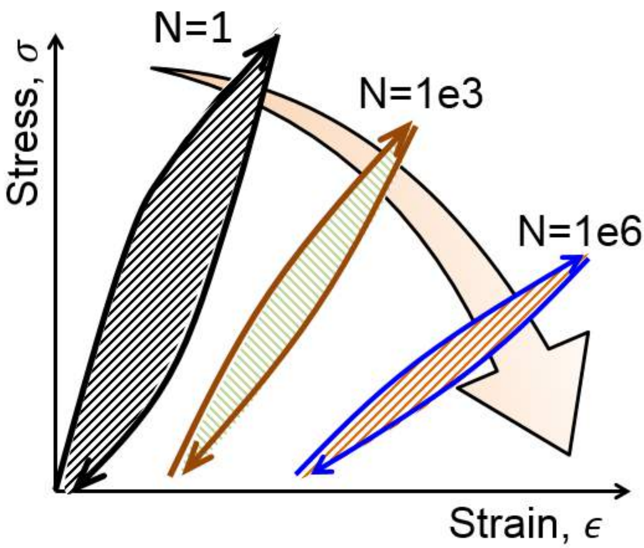

Figure 1 Cyclic hysteresis energy changes during cyclic loading a polymer system. Three effects are shown: (1) the fatigue damage mechanisms result in progressive loss of elastic properties, (2) the hysteresis energy changes due to progressive plasticity and damage interactions, and (3) the stress level is reduced because the elastic modulus will decrease at higher cycles.

1. Elastic, Plastic and Creep Constitutive Laws

It is assumed that infinitesimal deformation mechanisms govern the fatigue loading and the total strain rate tensor $\dot{\epsilon}_{ij}$ is partitioned into *undamaged* elastic rate $\dot{\bar{\epsilon}}_{ij}^{e}$, thermal strain rate $\dot{\epsilon}^{th}$, plastic strain rate $\dot{\epsilon}_{ij}^{p}$, creep strain rate $\dot{\epsilon}_{ij}^{c}$, and *damage* induced strain rate $\dot{\epsilon}_{ij}^{d}$ tensors,

$$\dot{\epsilon}_{ij} = \dot{\bar{\epsilon}}_{ij}^{e} + \dot{\epsilon}^{th}\delta_{ij} + \dot{\epsilon}_{ij}^{p} + \dot{\epsilon}_{ij}^{c} + \dot{\epsilon}_{ij}^{d} \tag{1}$$

where δ_{ij} is the Kronecker delta. The thermal expansion strain rate is given by $\dot{\epsilon}^{th} = \mathrm{A}\Delta T$ where A(T) is the *linear thermal expansion coefficient* that is a function of temperature and ΔT denotes the temperature difference between two time increments. The damage strain tensor $\epsilon_{ij}^{d} = \int \dot{\epsilon}_{ij}^{d} dt$ represents the additional elastic straining due to microcrack opening and closing effects [39-42].

The elasto-plastic, creep, and CDM model has been adopted from (Shojaei and Wedgewood, 2017) and the constitutive laws are only outlined in this section. The interested readers may refer to (Shojaei and Wedgewood, 2017) for more details.

- *Elastic Constitutive Model*

Although unfilled polymers are initially isotropic, they transform to an anisotropic material system due to damage propagation in different direction. For sake of simplicity, it is assumed the damaged material system obeys orthotropic elastic constitutive law [27, 43-45],

$$\begin{bmatrix} \dot{\sigma}_{11} \\ \dot{\sigma}_{22} \\ \dot{\sigma}_{33} \\ \dot{\sigma}_{12} \\ \dot{\sigma}_{23} \\ \dot{\sigma}_{31} \end{bmatrix} = \begin{bmatrix} C_{11} & C_{12} & C_{13} & & & \\ C_{12} & C_{22} & C_{23} & & 0 & \\ C_{13} & C_{23} & C_{33} & & & \\ & & & C_{44} & 0 & 0 \\ & 0 & & 0 & C_{55} & 0 \\ & & & 0 & 0 & C_{66} \end{bmatrix} \begin{bmatrix} \dot{\epsilon}_{11}^{e} \\ \dot{\epsilon}_{22}^{e} \\ \dot{\epsilon}_{33}^{e} \\ \dot{\epsilon}_{12}^{e} \\ \dot{\epsilon}_{23}^{e} \\ \dot{\epsilon}_{31}^{e} \end{bmatrix} \tag{2}$$

where C_{ij} is the *damaged* stiffness tensors, and $\dot{\sigma}_{ij}$ denotes the Cauchy stress rate.

- *Cyclic plasticity model*

Following [30, 31, 46], Chaboche's anisotropic plasticity flow rule with kinematic hardening is utilized to capture cyclic loading responses:

$$\dot{\epsilon}_{ij}^{p} = \frac{3}{2}\left|\dot{\epsilon}_{ij}^{p}\right| \frac{s_{ij}^{*}}{\sigma_{y}} \tag{3}$$

where $\left|\dot{\epsilon}_{ij}^{p}\right| = \sqrt{\frac{2}{3}\dot{\epsilon}_{ij}^{p}\dot{\epsilon}_{ij}^{p}}$ is the effective plastic strain rate and σ_y is the yield stress. The deviatoric stress s_{ij}^{*} is computed based on the following relation [30],

$$s_{ij}^{*} = s_{ij} - X_{ij} \tag{3}$$

where $X_{ij} = \alpha_{ij} - \frac{1}{3}\alpha_{kk}\delta_{ij}$ is the deviatoric part of the backstress tensor α_{ij} (to be defined later), and $s_{ij} = \sigma_{ij} - \frac{1}{3}\sigma_{kk}\delta_{ij}$ is the deviatoric Cauchy stress. The effective deviatoric stress, $\left|s_{ij}^{*}\right|$, is computed by [30],

$$\left|s_{ij}^{*}\right| = \sqrt{\frac{3}{2}s_{ij}^{*}s_{ij}^{*}} \tag{4}$$

Cyclic loading of unfilled polymer will result in ratcheting or shakedown, depending on the material system and the loading properties. In theory of plasticity kinematic and isotropic hardening constitutive laws are utilize to capture the ratcheting or shakedown phenomena. Chaboche's kinematic hardening relation is considered to model the hardening responses [30, 31, 46],

$$\dot{\alpha}_{ij} = \sum_{n=1}^{m}\left(\frac{2}{3}C_n\dot{\epsilon}_{ij}^{p} - \gamma_n\alpha_{ij}\left|\dot{\epsilon}_{ij}^{p}\right|\right) \tag{5}$$

where α_{ij} is deviatoric backstress tensor, and C_n and γ_n with $n = 1, \ldots, \mathrm{m}$ are material parameters. Chaboche's isotropic hardening law is utilized to capture cyclic changes in yield surface size [30, 31, 46]. The yield stress σ_y in Eq. (2) is defined as,

$$\sigma_y = \sigma_y^0 + R \tag{6}$$

where σ_y^0 is the initial yield strength, and R denotes the isotropic hardening effect,

$$\dot{R} = w(Q - R)|\dot{\epsilon}^{p}| \tag{7}$$

where w and Q are the material constants, and R is the accumulated amount of the incremental change of the yield surface. Then, $\sigma_y^0 + R$ represents the size of the yield surface at each cycle and R approaches to its asymptotic value through Eq. (17).

- *Creep Constitutive Laws:*

In the case of creep mechanisms, polymers and PMCs may undergo (i) *cohesion* creep, which is driven mainly by deviatoric part of applied stresses, and (ii) *volumetric swelling* that is a pressure driven phenomenon. Generally, creep models for cyclic loading are complicated and need to be introduced into FEA solvers through user-defined subroutines. In this work a simple power law relation is utilized to correlate the cyclic creep rate per cycle $\dot{\epsilon}_{ij}^{c}$ to the mean-stress σ_{ij}^{m},

$$\dot{\epsilon}_{ij}^{c} = A \times \left(\sigma_{ij}^{m}\right)^{\gamma} \times t^{\alpha} \tag{8}$$

where $\sigma_{ij}^{m} = 0.5 \times \left(\sigma_{ij}^{max} - \sigma_{ij}^{min}\right)$ indicates the mean-stress level, t (sec) denotes the creep period, and A, γ and α are material parameters. If cyclic creep, plasticity, and fatigue occur simultaneously, all behaviors may interact and a coupled system of constitutive equations needs to be solved.

- *Fatigue Damage Constitutive Laws:*

Damaged Young moduli E_i and Poisson's ratios v_i in 3 principal directions are updated based upon state of the damage in each principal directions, viz. D_i [27],

$$\begin{aligned} E_i &= \overline{E}(\delta_i - D_i) \\ v_i &= \overline{v}\left(\delta_i + D_i\left(\frac{0.5}{\overline{v}} - 1\right)\right) \end{aligned} \tag{9}$$

where $\overline{E}$ and $\overline{v}$ are elastic modulus and Poisson's ratio for the virgin polymer system, δ_i is the unit vector, and D_i denotes the damage tensor in 3 principal directions.

The CDM model needs to capture combined LCF and HCF damage effects in which statistical models are required to accounts for the different failure mechanisms in LCF and HCF processes. For sake of simplicity, the rule-of-mixture is utilized to control the contribution of LCF and HCF damaging mechanisms,

$$D_i = \zeta \times D_i^{LCF} + (1 - \zeta) \times D_i^{HCF} \tag{10}$$

where ζ is a loading characteristic and D_i^{LCF} and D_i^{HCF} denote LCF and HCF damage parameters, respectively. The loading characteristic parameter ζ is given by:

$$\zeta = \frac{(\sigma_{max} - S_e)}{(\sigma_u - S_e)} \tag{11}$$

where σ_u and S_e are ultimate and endurance stresses, respectively, and $S_e < \sigma_{max} < \sigma_u$ is the maximum stress in a cycle. Thus, for $\zeta = 0$ the HCF damage mechanisms dominate the fatigue failure, for $\zeta = 1$ the LCF damage mechanisms dominate the fatigue failure, and for $0 < \zeta < 1$ a linear combination of LCF and HCF damage mechanisms controls the lifetime.

The damage mechanisms in HCF corresponds to initiation and propagation of microcracks and the HCF damage parameter D_i^{HCF} is defined by,

$$D_i^{HCF} = \sum_{i=1}^{3} \frac{a_i - a_0}{a_{cr} - a_0} \tag{12}$$

where $a_i = \int \dot{a}_i dt$ is the microcrack length that is integrated in 3 principal directions, a_0 denotes initial microcrack length, and $a_{cr} \approx 1$(mm) represents the critical crack length in which unstable fracture occurs. On the other hand, the LCF damage mechanisms are governed by void nucleation and propagation. The damage parameter for LCF is then given by,

$$D_i^{LCF} = \sum_{i=1}^{3} \frac{V - V_0}{V_{cr} - V_0} \tag{13}$$

where $V_i = \int \dot{V}_i dt$ is microvoid volume growth, integrated in 3 principal directions that results in an elliptical void, V_0 represents the initial microvoid volume, and $V_{cr} \approx 1(mm^3)$ represents the critical void volume in which unstable fracture occurs.

The constitutive relation for computation of the microcrack length growth rate $\dot{a}_i$ and microvoid volume growth rate $\dot{V}_i$ can be developed based upon cyclic stress, strain or hysteresis energy concepts. The most promising approach for calibrating the CDM fatigue model is to use directly measured S-N or E-N data to develop the constitutive laws. In order to reproduce S-N data, a partitioning method for the stress is adopted herein. The S-N data needs to be curve-fit to feed into the computational tool. Any complex S-N data in polymers can be fit by splitting the life space into $N < N_{split}$ and $N \geq N_{split}$ as follows,

$$S^{(T)} = \begin{cases} C_{ee}^{(T)} N^{A_{ee}^{(T)}} + C_{pp}^{(T)} N^{A_{pp}^{(T)}} & \text{for } N > N_{split} \\ \dfrac{S_0^{(T)} - S_{N_{split}}^{(T)}}{1 - N_{split}^{(T)}} \left(N - N_{split}^{(T)}\right) + S_{N_{split}}^{(T)} & \text{for } N < N_{split} \end{cases} \tag{14}$$

where superscript "(T)" denotes the temperature, parameter $S_0^{(T)}$ is the reference quasi-static strength at T, $S_{N_{split}}^{(T)}$ is calculated strength by setting $N = N_{split}$ is Eq. $(24)_1$. The first equation in Eq. $(24)_1$ is basically a simple *stress partitioning* law, where $C_{ee}^{(T)}$ (MPa), $A_{ee}^{(T)}$, $C_{pp}^{(T)}$ (MPa), and $A_{pp}^{(T)}$ are all curve fitting parameters for temperature T. The values of $C_{ee}^{(T)}$ and C_{pp}^{T} can be approximated directly found from S-N data in which $C_{ee}^{(T)} = S_e^{(T)}$ is the endurance limit at temperature T and $C_{pp}^{(T)} = S_0^{(T)} - S_e^{(T)}$.

2. Computational Implementation

The CDM-FEA framework is implemented into a Abaqus through user-defined coding, i.e. UMAT. The developed damage variables are updated cyclically at each material point as field variables and the updated values are utilized to reduce the elastic tensile and shear moduli in 3 principal directions. Once the damage parameter reaches to its critical value in the integration points, the corresponding stiffness is set to a small value to artificially remove the respective element from the model. A unique feature of the developed fatigue computational platform is the combination of cyclic creep and cyclic fatigue damage in which the history of fatigue and creep phenomena is captured and is considered for the next time increment.

3. RESULTS AND DISCUSSION:

DuPont™ Delrin® acetal homopolymer resin is a highly-crystalline engineering thermoplastic polymer particularly suited for high load mechanical applications, such as gears, safety restraints, door systems, conveyor belts, healthcare delivery devices and components across a diverse range of products and industries. The performance of the developed computational platform is investigated for fatigue life prediction and self-heating effects of Delrin®. Density of Delrin 100 is about 1420 (Kg/m^3), coefficient of thermal conductivity is in the range of 0.3 to 0.37 (W/m ^{o}C), and its specific heat is assumed to be 1100 (J/Kg ^{o}C).

Figures 3 (a) and (b) show the elasto-plastic response of Delrin100 at 23^{o}C and 60^{o}C, respectively, in which Chaboche's plasticity model is used to simulate a deformation controlled cyclic loading, $\epsilon_{min} = 0\%$ and $\epsilon_{max} = 50\%$.

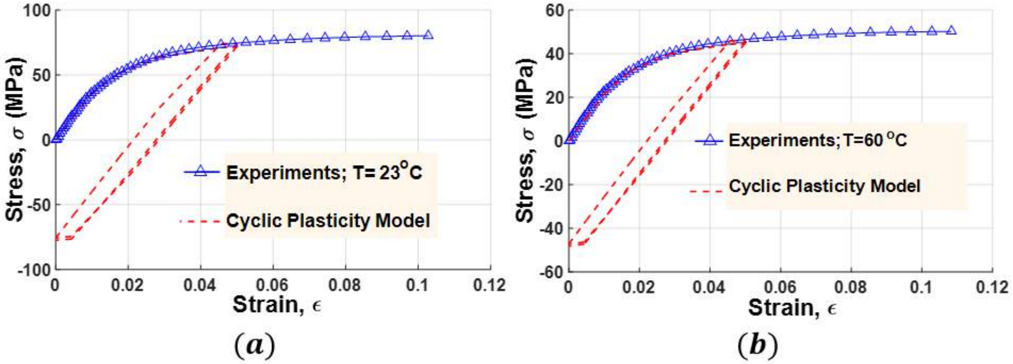

Figure 2 Delrin® 100 elasto-plastic response and plasticity model performance under deformation controlled cyclic loading at (a) temperature is 23^{o}C and the undamaged Young modulus is $\bar{E} \approx 3100$ (MPa), and undamaged Poisson's ratio is $\bar{\nu} = 0.3$, and (b) T= 60^{o}C, $\bar{E} \approx 2000$ (MPa), and $\bar{\nu} = 0.3$.

The cyclic plasticity and CDM models are utilized to replicate the S-N data points for both 23^{o}C and 60^{o}C cases. Figures 3(a) and (b) illustrate respectively the performance of calibrated CDM model in capturing S-N curves at 23^{o}C and 60^{o}C. Other CDM model parameters are listed in Table 1. The S-N models for 23°C and 60°C are shown by solid blue lines and the model parameters are listed in Table 2.

Table 1 CDM Model parameters for Delrin®100

a_{cr} (mm)	a_0 (mm)	V_{cr} (mm^3)	V_0 (mm^3)	ϵ_f (%)
1	0	1	0	15

Table 2 S-N model parameters for Delrin®100 at 23^{o}C and 60^{o}C (*f*= *1(Hz)*, and *R=0.1*)

$\boldsymbol{T}$ (°C)	$\boldsymbol{C_{ee}}$ $(\boldsymbol{MPa})$	$\boldsymbol{A_{ee}}$	$\boldsymbol{C_{pp}}$ $(\boldsymbol{MPa})$	$\boldsymbol{A_{pp}}$	$\boldsymbol{N_{split}}$
23	51	-0.01	68-C_{ee}	-0.6	5000
60	46	-0.005	53-C_{ee}	-0.2	1000

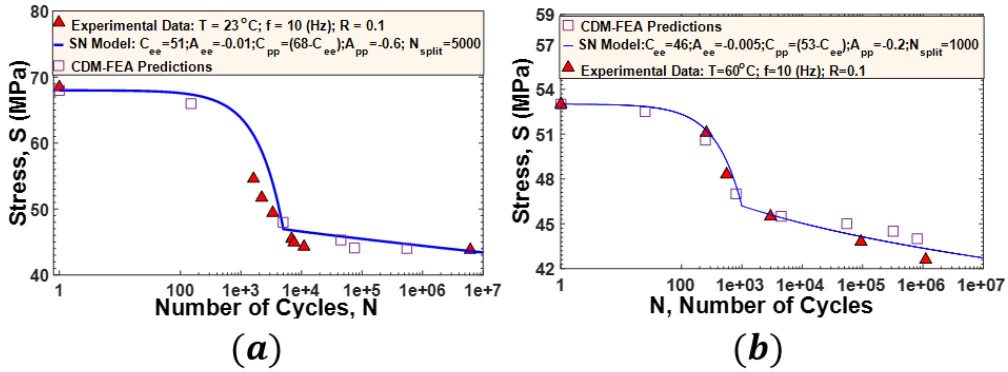

Figure 3 Delrin® 100 S-N curve at (a) T=23°C and (b) T=60°C. Fatigue experiments have been conduced at 10Hz loading. The S-N model is utilized to curve fit the experiments (blue line). The curve fit S-N model is then introduced to the CDM-FEA computational tool to predict the fatigue life. CDM-FEA model correlates well with the experimental data.

For sake of simplicity, linear correlations are utilized herein to link the frequency and stress effects and self-heating.

$$F(f) = \eta_0^f + \frac{\eta_1^f - \eta_0^f}{f_1 - f_0}(f - f_0),$$
$$G(\sigma^{max}) = \eta_0^\sigma + \frac{\eta_1^\sigma - \eta_0^\sigma}{\sigma_1 - \sigma_0}(\sigma - \sigma_0). \tag{15}$$

where η_0^f and η_1^f are dissipation coefficients at f_0 and f_1 frequencies, respectively, and η_1^σ and η_0^σ are coefficients at σ_1 and σ_0, maximum stress levels, respectively. Table 3 summarizes the values for these coefficients for the simulation results that are shown in Fig 4(a).

Table 3 Empirical coefficients for frequency and max stress effects on self-heating

f (Hz)	$\frac{\sigma^{max}}{\sigma^u}$	η_0^f (%)	η_1^f (%)	η_0^σ (%)	η_1^σ (%)
1	0.65	6.0	-	-	-
5	0.65	-	6.8	6.8	-
5	0.9	-	-	-	8.0

As reported by Vallance et al. [50], frequency, load amplitude, and number of cycles can all affect the self-heating in Delrin® 100, see Fig. 5. Figure 4(a) shows the effect of frequency on temperature rise at stabilized cycles in which simulation results correlates well with the reported temperature rises, by Vallance et al.[50]. Figure 4(b) indicates that the transient nature of the self-heating effect in which temperature is stabilized at certain cycle number. The maximum applied load level on the sample also contributes to the temperature rise, as depicted in Fig. 4(c).

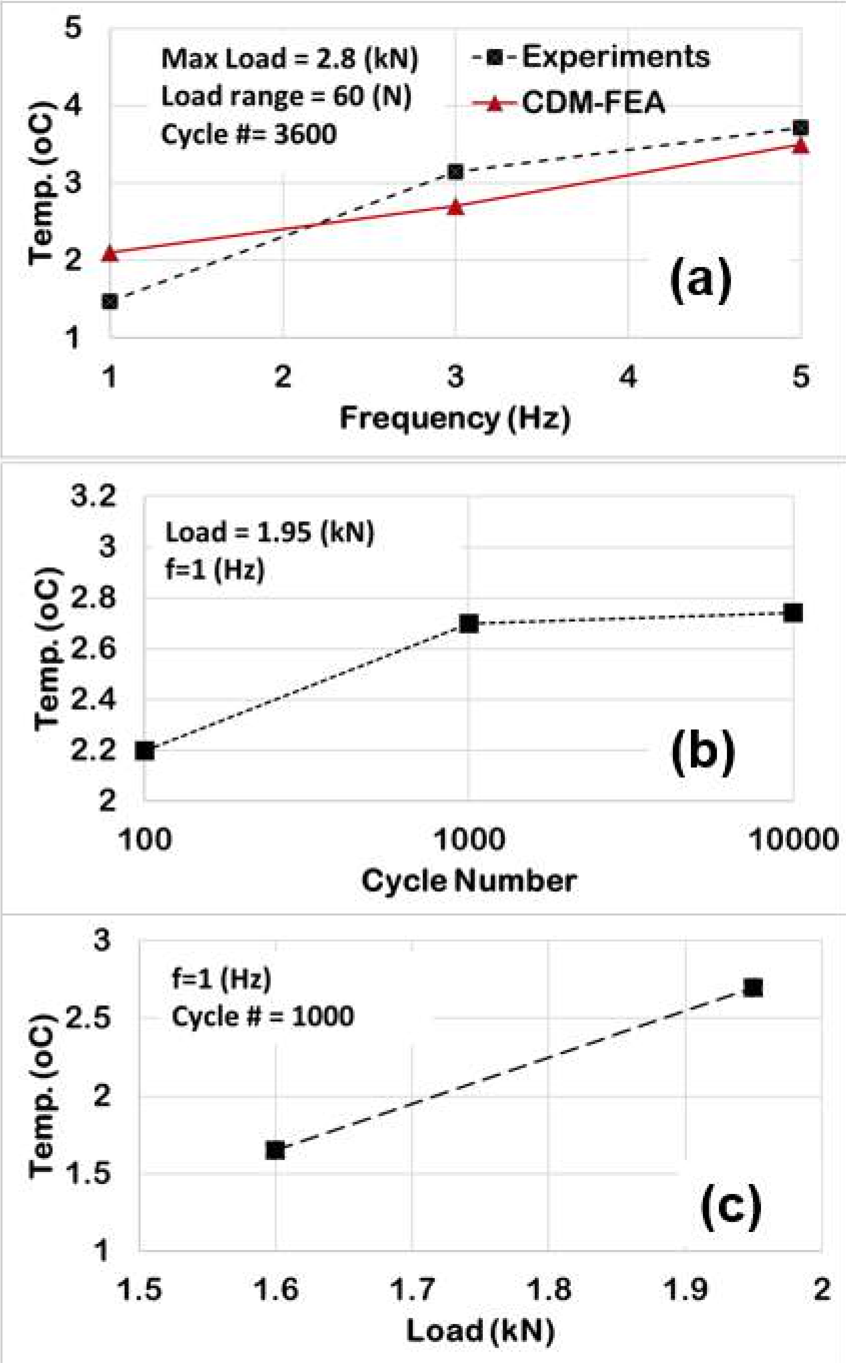

Figure 4 Effect of (a) frequency, (b) number of cycles, and (c) load amplitude on the self-heating phenomenon in Delrin® 100. Experiments are after [50].

ISO-3167 bar is subjected to the 2.8-0.06 (kN) cyclic loads with 1 (Hz) frequency in Fig. 5. The calculated temperature rises, using the proposed coupled CDM-FEA method, correlate well with the reported experimental data in Fig. 4(a).

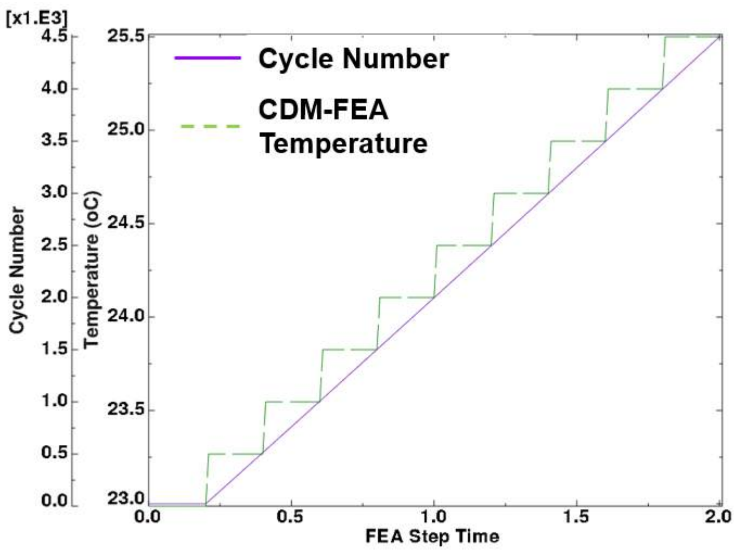

Figure 5 ISO-3167 bar is subjected to the 2.8-0.06 (kN) cyclic loads with 1 (Hz) frequency. CDM-FEA simulation for temperature rise in Delrin® 100. The simulation results correlate well with the experimental data, shown in Fig. 5(a).

The next case study is Delrin® self-heating effects in a 50×100×2mm open-hole sample with a 10mm central hole. Figure 5 depicts the FEA problem in which an open hole sample is loaded cyclically. The mechanical dissipation mechanisms are converted into heat generation in each element. The thermal problem considers both a conductive (within the sample) and a convective (between sample and air) heat transfer mechanism to calculate the temperature at each element.

Figure 6 shows an open hole sample, subjected to a stress-controlled cyclic loading, viz. 0-35 (MPa). Temperature, damage and plastic strain for different cycles are depicted. At $N=500$ the fatigue damage is initiated and at $N=2500$ and $N=3000$ an inclined crack is formed. The temperature rises due to progressive fatigue damage and cyclic plasticity effects are shown at $N=500$, *2500*, and *3000* cycles.

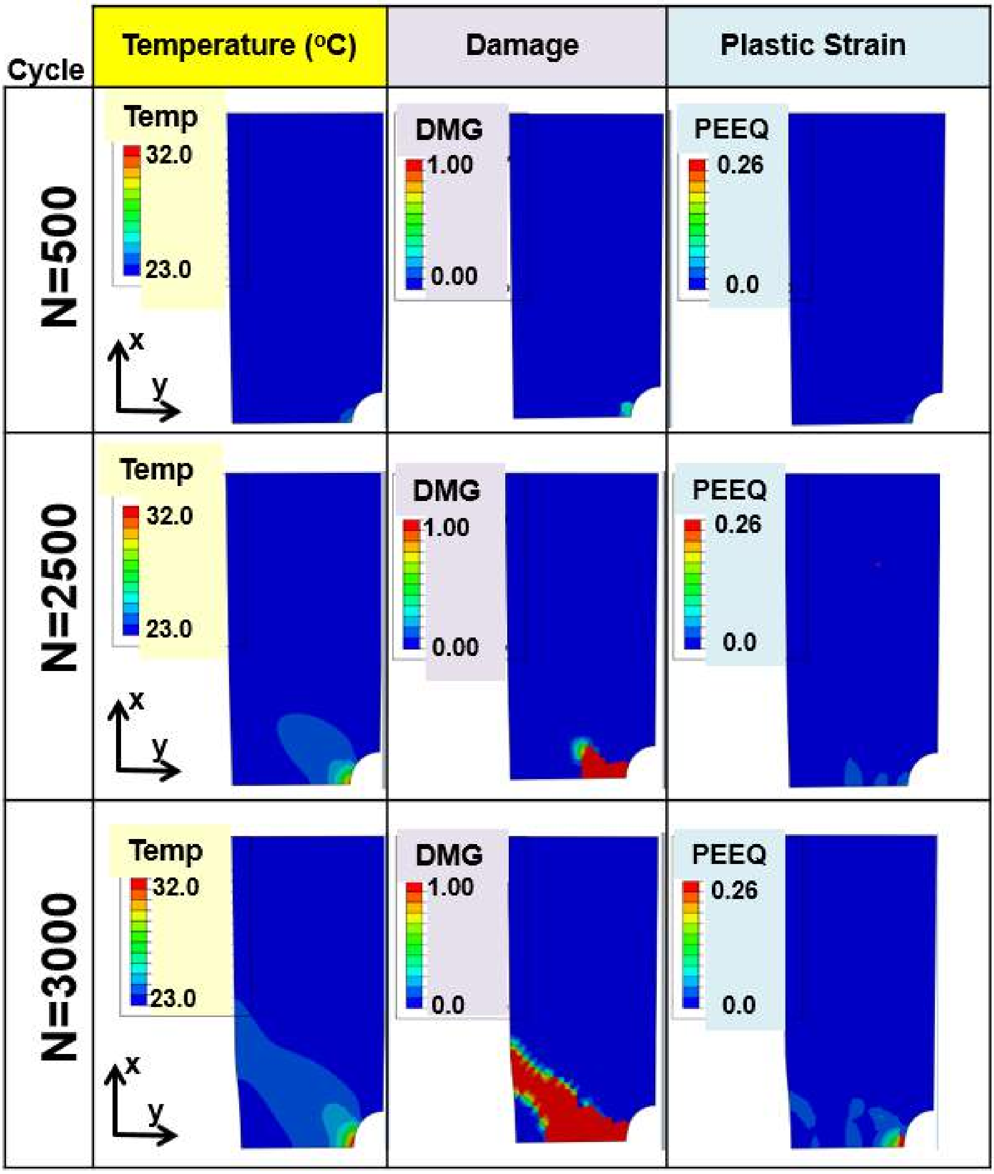

Figure 6 Abaqus simulation: An open-hole Delrin® 100 NC010 sample under 0-35 (MPa) stress-controlled cyclic loading. The graph shows the effects of progressive damage and cyclic plastic on self-heating.

4. Concluding Remarks

The effects of self-heating on fatigue life of polymer and PMC systems are investigated. The thermodynamic principles are utilized to link cyclic hysteresis energy to the heat buildup effects. It is shown that the CDM-FEA model can capture the self-heating effect and the simulations results correlates well with observed experimental data.

5. Acknowledgment

This work was supported by DuPont Performance Materials (DPM).

References

[1] Launay, A., Y. Marco, M.H. Maitournam, and I. Raoult, *Modelling the influence of temperature and relative humidity on the time-dependent mechanical behaviour of a short glass fibre reinforced polyamide.* Mechanics of Materials, 2013b. **56**: p. 1-10.

[2] Mortazavian, S. and A. Fatemi, *Fatigue behavior and modeling of short fiber reinforced polymer composites including anisotropy and temperature effects.* International Journal of Fatigue, 2015. **77**: p. 12-27.

[3] Fries, T.-P. and T. Belytschko, *The extended/generalized finite element method: An overview of the method and its applications.* International Journal for Numerical Methods in Engineering, 2010. **84**(3): p. 253-304.

[4] Curiel Sosa, J.L. and N. Karapurath, *Delamination modelling of GLARE using the extended finite element method.* Composites Science and Technology, 2012. **72**(7): p. 788-791.

[5] Ferté, G., P. Massin, and N. Moës, *3D crack propagation with cohesive elements in the extended finite element method.* Computer Methods in Applied Mechanics and Engineering, 2016. **300**: p. 347-374.

[6] Giner, E., C. Navarro, M. Sabsabi, M. Tur, J. Domínguez, and F.J. Fuenmayor, *Fretting fatigue life prediction using the extended finite element method.* International Journal of Mechanical Sciences, 2011. **53**(3): p. 217-225.

[7] Giner, E., N. Sukumar, F.D. Denia, and F.J. Fuenmayor, *Extended finite element method for fretting fatigue crack propagation.* International Journal of Solids and Structures, 2008. **45**(22–23): p. 5675-5687.

[8] Pourmodheji, R. and M. Mashayekhi, *Improvement of the extended finite element method for ductile crack growth.* Materials Science and Engineering: A, 2012. **551**: p. 255-271.
[9] Sadeghirad, A., D.L. Chopp, X. Ren, E. Fang, and J. Lua, *A novel hybrid approach for level set characterization and tracking of non-planar 3D cracks in the extended finite element method.* Engineering Fracture Mechanics, 2016. **160**: p. 1-14.
[10] Sharafisafa, M. and M. Nazem, *Application of the distinct element method and the extended finite element method in modelling cracks and coalescence in brittle materials.* Computational Materials Science, 2014. **91**: p. 102-121.
[11] Xu, Y. and H. Yuan, *Computational analysis of mixed-mode fatigue crack growth in quasi-brittle materials using extended finite element methods.* Engineering Fracture Mechanics, 2009. **76**(2): p. 165-181.
[12] Borg, R., L. Nilsson, and K. Simonsson, *Simulation of delamination in fiber composites with a discrete cohesive failure model.* Composites Science and Technology, 2001. **61**(5): p. 667-677.
[13] Li, H. and N. Chandra, *Analysis of crack growth and crack-tip plasticity in ductile materials using cohesive zone models.* International Journal of Plasticity, 2003. **19**(6): p. 849-882.
[14] Zhang, Z. and G.H. Paulino, *Cohesive zone modeling of dynamic failure in homogeneous and functionally graded materials.* International Journal of Plasticity, 2005. **21**(6): p. 1195-1254.
[15] Chaboche, J.L., R. Girard, and P. Levasseur, *On the Interface Debonding Models.* International Journal of Damage Mechanics, 1997. **6**(3): p. 220-257.
[16] Bouvard, J.L., J.L. Chaboche, F. Feyel, and F. Gallerneau, *A cohesive zone model for fatigue and creep–fatigue crack growth in single crystal superalloys.* International Journal of Fatigue, 2009. **31**(5): p. 868-879.
[17] Paranjape, H.M., S. Manchiraju, and P.M. Anderson, *A phase field – Finite element approach to model the interaction between phase transformations and plasticity in shape memory alloys.* International Journal of Plasticity, 2016. **80**: p. 1-18.
[18] Ding, F., M. Feng, and Y. Jiang, *Modeling of fatigue crack growth from a notch.* International Journal of Plasticity, 2007. **23**(7): p. 1167-1188.
[19] Hazeli, K., H. Askari, J. Cuadra, F. Streller, R.W. Carpick, H.M. Zbib, and A. Kontsos, *Microstructure-sensitive investigation of magnesium alloy fatigue.* International Journal of Plasticity, 2015. **68**: p. 55-76.

[20] Kang, G., Y. Liu, J. Ding, and Q. Gao, *Uniaxial ratcheting and fatigue failure of tempered 42CrMo steel: Damage evolution and damage-coupled visco-plastic constitutive model.* International Journal of Plasticity, 2009. **25**(5): p. 838-860.

[21] Moreo, P., J.M. García-Aznar, and M. Doblaré, *A coupled viscoplastic rate-dependent damage model for the simulation of fatigue failure of cement–bone interfaces.* International Journal of Plasticity, 2007. **23**(12): p. 2058-2084.

[22] Pirondi, A., N. Bonora, D. Steglich, W. Brocks, and D. Hellmann, *Simulation of failure under cyclic plastic loading by damage models.* International Journal of Plasticity, 2006. **22**(11): p. 2146-2170.

[23] Voyiadjis, G.Z., A. Shojaei, and G. Li, *A thermodynamic consistent damage and healing model for self healing materials.* International Journal of Plasticity, 2011. **27**(7): p. 1025-1044.

[24] Voyiadjis, G.Z., A. Shojaei, G. Li, and P.I. Kattan, *A theory of anisotropic healing and damage mechanics of materials.* Proceedings of the Royal Society A: Mathematical, Physical and Engineering Science, 2012a. **468**(2137): p. 163-183.

[25] Shojaei, A. and G. Li, *Thermomechanical constitutive modelling of shape memory polymer including continuum functional and mechanical damage effects.* Proceedings of the Royal Society of London A: Mathematical, Physical and Engineering Sciences, 2014. **470**(2170).

[26] Shojaei, A., *Modeling of self-healing smart composite materials*, in *Recent Advances in Smart Self-healing Polymers and Composites*, H. Meng and G. Li, Editors. 2015a, Woodhead Publishing. p. 21-52.

[27] Shojaei, A., G. Li, P.J. Tan, and J. Fish, *Dynamic delamination in laminated fiber reinforced composites: A continuum damage mechanics approach.* International Journal of Solids and Structures, 2015c. **71**: p. 262-276.

[28] Murakami, S., *A continuum mechanics theory of anisotropic damage. In: Yielding, damage, and failure of anisotropic solids.* proceedings of the IUTAM/ICM symposium, EGF publication, vol. 5, pp. 465-482., 1990.

[29] Abu Al-Rub, R.K. and G.Z. Voyiadjis, *On the coupling of anisotropic damage and plasticity models for ductile materials.* International Journal of Solids and Structures, 2003. **40**(11): p. 2611-2643.

[30] Chaboche, J.L., *On some modifications of kinematic hardening to improve the description of ratchetting effects.* International Journal of Plasticity, 1991. **7**(7): p. 661-678.
[31] Chaboche, J.L., *A review of some plasticity and viscoplasticity constitutive theories.* International Journal of Plasticity, 2008. **24**(10): p. 1642-1693.
[32] Shojaei, A., M. Eslami, and H. Mahbadi, *Cyclic loading of beams based on the Chaboche model.* International Journal of Mechanics and Materials in Design, 2010. **6**(3): p. 217-228.
[33] Chaboche, J.L., P. Kanouté, and F. Azzouz, *Cyclic inelastic constitutive equations and their impact on the fatigue life predictions.* International Journal of Plasticity, 2012. **35**(0): p. 44-66.
[34] Mahbadi, H., A. Shojaei, and M. Eslami, *Thermal Cyclic Loading of Beams Based on the Chaboche Kinematic Hardening Model*, in *Encyclopedia of Thermal Stresses*, R. Hetnarski, Editor. 2014, Springer Netherlands. p. 4968-4974.
[35] Bari, S. and T. Hassan, *An advancement in cyclic plasticity modeling for multiaxial ratcheting simulation.* International Journal of Plasticity, 2002. **18**(7): p. 873-894.
[36] Bari, S. and T. Hassan, *Kinematic hardening rules in uncoupled modeling for multiaxial ratcheting simulation.* International Journal of Plasticity, 2001. **17**(7): p. 885-905.
[37] Bari, S. and T. Hassan, *Anatomy of coupled constitutive models for ratcheting simulation.* International Journal of Plasticity, 2000. **16**(3–4): p. 381-409.
[38] Bonnand, V., J.L. Chaboche, P. Gomez, P. Kanouté, and D. Pacou, *Investigation of multiaxial fatigue in the context of turboengine disc applications.* International Journal of Fatigue, 2011. **33**(8): p. 1006-1016.
[39] Shojaei, A., G. Li, and G.Z. Voyiadjis, *Cyclic Viscoplastic-Viscodamage Analysis of Shape Memory Polymers Fibers With Application to Self-Healing Smart Materials.* Journal of Applied Mechanics, 2012. **80**(1): p. 1-15.
[40] Voyiadjis, Z. and P.I. Kattan, *Advances in Damage Mechanics*. 2006, London: Elsevier.
[41] Lemaitre, J. and J.L. Chaboche, *Mechanics of Solid Materials*. 1990, Cambridge: Cambridge University Press.
[42] Lemaitre, J., *A Course on Damage Mechanics*. 1992: Springer-Verlag, Berlin.

[43] Shao, J.F., *Poroelastic behaviour of brittle rock materials with anisotropic damage.* Mechanics of Materials, 1998. **30**(1): p. 41-53.

[44] Shojaei, A. and J. Fish, *Assessment of Reduced Order Homogenization for Damage Tolerant Design Principles (DTDP) of Advanced Composite Aircraft Structures*, in *56th AIAA/ASCE/AHS/ASC Structures, Structural Dynamics, and Materials Conference*. 2015, American Institute of Aeronautics and Astronautics.

[45] Shojaei, A., G. Li, J. Fish, and P.J. Tan, *Multi-scale Constitutive Modeling of Ceramic Matrix Composites by Continuum Damage Mechanics.* International Journal of Solids and Structures, 2014. **51**(23-24): p. 4068-4081.

[46] Chaboche, J.L., *Thermodynamic formulation of constitutive equations and application to the viscoplasticity and viscoelasticity of metals and polymers.* International Journal of Solids and Structures, 1997. **34**(18): p. 2239-2254.

[47] Lemaitre, J. and J. Dufailly, *Damage measurements.* Engineering Fracture Mechanics, 1987. **28**(5-6): p. 643-661.

[48] Lemaitre, J., *Coupled elasto-plasticity and damage constitutive equations.* Computer Methods in Applied Mechanics and Engineering, 1985. **51**(1-3): p. 31-49.

[49] Lemaitre, J., *How to use damage mechanics.* Nuclear Engineering and Design, 1984. **80**(2): p. 233-245.

[50] Vallance, L., *The Influence of Temperature on Damage Accumulation in Cyclically-loaded Non-reinforced Engineering Plastics*. 2014, Master Thesis, University of Sheffield, Sheffield, UK.

[51] Amir K. Shojaei, Alan R. Wedgewood, An anisotropic cyclic plasticity, creep and fatigue predictive tool for unfilled polymers, Mechanics of Materials, Volume 106, March 2017, Pages 20-34, ISSN 0167-6636, http://dx.doi.org/10.1016 j.mechmat.2017.01.003.